Multiple Sulfur Isotope Records of the 3.22 Ga Moodies Group, Barberton Greenstone Belt

Masafumi Saitoh, Sami Nabhan, Christophe Thomazo, Nicolas Olivier, Jean-François Moyen, Yuichiro Ueno, Johanna Marin-Carbonne

geosciences

MDPI

Article

Multiple Sulfur Isotope Records of the 3.22 Ga Moodies Group, Barberton Greenstone Belt

Masafumi Saitoh [1,2,*], Sami Nabhan [3], Christophe Thomazo [4], Nicolas Olivier [1], Jean-François Moyen [5], Yuichiro Ueno [6,7] and Johanna Marin-Carbonne [2]

1 Laboratoire Magmas et Volcans, CNRS, Université Clermont Auvergne, 63170 Aubière, France; Nicolas.olivier@uca.fr
2 Institut des Sciences de la Terre, Université de Lausanne, 1015 Lausanne, Switzerland; johanna.marincarbonne@unil.ch
3 Institut de Physique du Globe de Paris, CNRS, Université de Paris, 75238 Paris, France; nabhan@ipgp.fr
4 Laboratoire Biogéosciences, Université Bourgogne Franche-Comté, 25000 Besançon, France; christophe.thomazo@u-bourgogne.fr
5 Laboratoire Magmas et Volcans, UJM-UCA-CNRS-IRD, Université de Lyon, 42023 Saint-Étienne, France; jean.francois.moyen@univ-st-etienne.fr
6 Department of Earth and Planetary Sciences, Tokyo Institute of Technology, Tokyo 152-8550, Japan; ueno.y.ac@m.titech.ac.jp
7 Earth-Life Science Institute, Tokyo Institute of Technology, Tokyo 152-8550, Japan
* Correspondence: masafumi.saitoh@unil.ch; Tel.: +41-21-692-4436

Received: 31 January 2020; Accepted: 13 April 2020; Published: 16 April 2020

Abstract: The Moodies Group, the uppermost unit in the Barberton Greenstone Belt (BGB) in South Africa, is a ~3.7-km-thick coarse clastic succession accumulated on terrestrial-to-shallow marine settings at around 3.22 Ga. The multiple sulfur isotopic composition of pyrite of Moodies intervals was newly obtained to examine the influence of these depositional settings on the sulfur isotope record. Conglomerate and sandstone rocks were collected from three synclines north of the Inyoka Fault of the central BGB, namely, the Eureka, Dycedale, and Saddleback synclines. The sulfur isotopic composition of pyrite was analyzed by Secondary Ion Mass Spectrometry (SIMS) for 6 samples from the three synclines and by Isotope Ratio Mass Spectrometry (IR-MS) for 17 samples from a stratigraphic section in the Saddleback Syncline. The present results show a signal of mass-independent fractionation of sulfur isotopes (S-MIF), although t-tests statistically demonstrated that the Moodies S-MIF signals (mostly 0‰ < $\Delta^{33}S$ < +0.5‰) are significantly small compared to the signal of the older Paleoarchean (3.6–3.2 Ga) records. These peculiar signatures might be related to initial deposition of detrital pyrite of juvenile origin from the surrounding intrusive (tonalite–trondhjemite–granodiorite; TTG) and felsic volcanic rocks, and/or to secondary addition of hydrothermal sulfur during late metasomatism. Moreover, fast accumulation (~0.1–1 mm/year) of the Moodies sediments might have led to a reduced accumulation of sulfur derived from an atmospheric source during their deposition. As a result, the sulfur isotopic composition of the sediments may have become susceptible to the secondary addition of metasomatic sulfur on a mass balance point of view. The sulfur isotopic composition of Moodies pyrite is similar to the composition of sulfides from nearby gold mines. It suggests that, after the Moodies deposition, metasomatic pyrite formation commonly occurred north of the Inyoka Fault in the central BGB at 3.1–3.0 Ga.

Keywords: Barberton; paleoarchean; Moodies Group; pyrite; quadruple sulfur isotopes; SIMS; IR-MS

1. Introduction

The 3.22 Ga, ~3.7-km-thick Moodies Group forms the stratigraphically uppermost part of the Barberton Greenstone Belt (BGB) in South Africa (e.g., [1]). The Moodies Group is suggested to be one of the oldest terrestrial-to-shallow marine transitional units in the geological record (e.g., [2,3]). This group is mainly composed of medium-to-coarse-grained sandstone [4,5]. Heubeck et al. (2013) estimated that the Moodies Group accumulated rapidly at rates of ca. 0.1 to 1 mm / year within <1 to 14 Ma using zircon U-Pb isochrones [6]. The quartz-rich siliciclastic sands, conglomerates, and silts accumulated on terrestrial to shallow-marine settings, reflecting alluvial, coastal flood plain and intertidal to subtidal depositional environments [5].

Abundant fossilized microbial mats have been reported, mostly from tidal and alluvial environments of the Moodies Group. Noffke et al. (2006) first proposed that wrinkle and roll-up sedimentary structures in the Moodies are microbially induced sedimentary structures (MISS) that had formed due to active microbial mats [7]. Heubeck (2009) subsequently interpreted that ubiquitous anastomosing branching and wavy laminations in the Moodies sandstones were remnants of microbial mats [8]. Homann et al. (2015) finally classified the laminae into three morphotypes and suggested a direct relationship between the mat morphologies and their associated depositional environments where planar-type lamina was a characteristic of coastal floodplain environments [9]. Wavy- and tufted-types typically formed in intertidal and in upper inter- to supra-tidal settings, respectively. Bulk carbon and nitrogen isotopic composition of organic remains has been reported on a deepening-upward fluvial to tidal succession of conglomerate and sandstone in the Dycedale Syncline and on a tidal sandstone succession in the Saddleback Syncline of the central BGB (Figure 1) [10]. A systematic difference in the carbon and nitrogen isotopic composition between the Moodies terrestrial and marine strata was observed and interpreted to reflect the oldest evidence for the co-existence of a distinctive land and marine biosphere. As well as carbon and nitrogen, sulfur is a major element in the biogeochemical cycles in the ocean/atmosphere system, and sulfur isotopes are well known as a useful tool to trace the past sulfur cycle [11]. The sulfur cycle and the search for a possible sulfur isotopic biosignature in the Moodies rocks have however not yet been addressed in previous studies [12,13].

The Archean rock record is characterized by the retention of mass-independent fractionation of sulfur isotopes (S-MIF) [14,15]. Sulfur has four stable isotopes (^{32}S, ^{33}S, ^{34}S, and ^{36}S) and a capital delta value is defined as a deviation from a mass-dependent fractionation (MDF) relationship using the following system of equations (e.g., [16]):

$$\Delta^{33}S = \delta^{33}S - ((1 + \delta^{34}S)^{0.515} - 1) \times 1000, \quad (1)$$

And

$$\Delta^{36}S = \delta^{36}S - ((1 + \delta^{34}S)^{1.90} - 1) \times 1000, \quad (2)$$

where

$$\delta^{x}S = (({}^{x}S/{}^{32}S)_{sample}/({}^{x}S/{}^{32}S)_{reference} - 1) \times 1000\ (‰)\ (x = 33, 34, \text{and } 36). \quad (3)$$

Generally, the $\Delta^{33}S$ value depends on the degree of $\delta^{34}S$ fractionation [11], and a recent study proposed a S-MIF threshold considering this dependency [17]. We use the S-MIF threshold in the following. Photochemical reactions of sulfur dioxide (SO_2) in the reducing atmosphere have been proposed to be the main S-MIF yielding mechanism for the Archean sulfur isotope record [14]. Laboratory experiments have demonstrated that elemental sulfur (S^0) with positive $\Delta^{33}S$ value and sulfate with negative $\Delta^{33}S$ value are produced during photochemical reactions of SO_2 (e.g., [18–20]). Nonetheless, detailed S-MIF generation pathways are still debated (e.g., [21]).

Ono et al. (2009) suggested that lithofacies of the host sediments is a controlling factor on the quadruple sulfur isotope record from the Neoarchean (2.8–2.5 Ga) Transvaal Supergroup, South Africa [22]. The authors suggested that early carbonate cementation turned the initial microbial sediments into a closed system where the sedimentary sulfur cycle was largely controlled by microbial

sulfate reduction (MSR). This example demonstrates that a lithofacies-controlled post-depositional process can substantially influence the sulfur isotope record of sediments. However, such an influence of the lithology and related early post-depositional processes on the sulfur isotope record have not yet been examined in detail in the older Paleoarchean (3.6–3.2 Ga) record. Here we explore the multiple sulfur isotopic composition of pyrite from the Moodies Group and examine the relationship between the characteristic depositional setting and lithofacies, post-depositional processes, and the sulfur isotope records, of the Moodies sediments.

2. Geologic Setting

The BGB is located in northeastern South Africa and northern Eswatini (Swaziland) near the eastern margin of the Kaapvaal Craton (Figure 1a). It is one of the best-preserved Paleoarchean greenstone belts and consists of a >10-km-thick succession of interlayered volcanic and sedimentary rocks, termed the Barberton Supergroup (e.g., [4,23]). The Barberton Supergroup (ca. 3.55 to 3.22 Ga) is subdivided (in ascending order) into the Onverwacht, the Fig Tree, and the Moodies groups. The Onverwacht Group (ca. 3.55 to 3.26 Ga) is mainly composed of mafic to ultramafic volcanic rocks (basalts and komatiites) with interlayered cherts and rare felsic volcanics as well as very few clastic units. The lithologically diverse Fig Tree Group (ca. 3.26 to 3.23 Ga) includes clastic sedimentary rocks (shales, sandstones and conglomerates), immature volcaniclastics, intermediate to felsic lavas, banded iron formations, barite, and cherts. The Moodies Group (ca. 3.22 Ga) is ~3.7 km thick and consists mainly of quartz-rich sandstones and siltstones with subordinate conglomerates, felsic volcanics, shales, and jaspilites [24]. The BGB is tightly folded; the central belt consists of a series of synclines, mostly cored by Moodies Group strata and separated by strike faults replacing tight anticlines [24,25]. The Inyoka Fault is one of these faults and a major divide in the BGB.

North of the Inyoka Fault, the Moodies Group is exposed in several tectonic units, including (from northeast to southwest) the Eureka Syncline, Dycedale Syncline, Saddleback Syncline, Moodies Hills Block, and Stolzburg Syncline (Figure 1) (e.g., [9,25–27]). The Eureka Syncline exposes Moodies strata of ~3.2 km thickness and has been subdivided in fair detail. The adjacent Dycedale Syncline exposes at least 600 m of Moodies strata [5,28]. The Saddleback Syncline exposes a ~3.5-km-thick complete Moodies section from the basal conglomerates (MdB unit) to the uppermost quartzarenites (MdQ3 unit) and conglomerates (MdQ3cgl unit) [9,28].

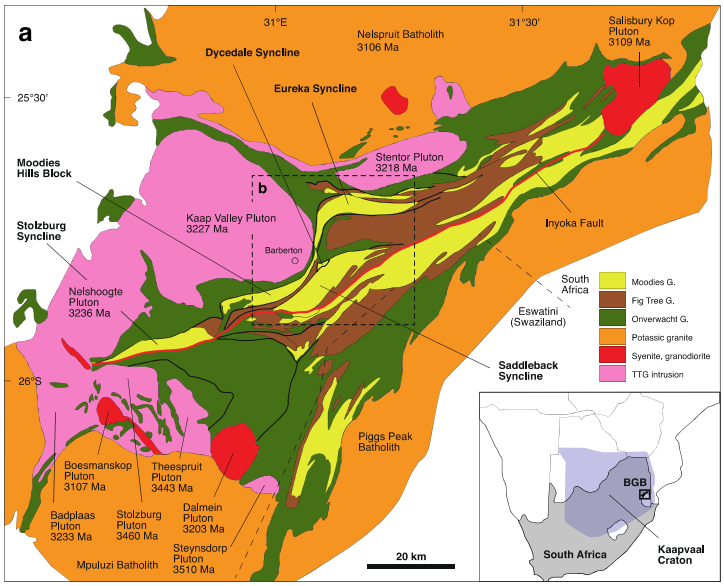

Figure 1. *Cont.*

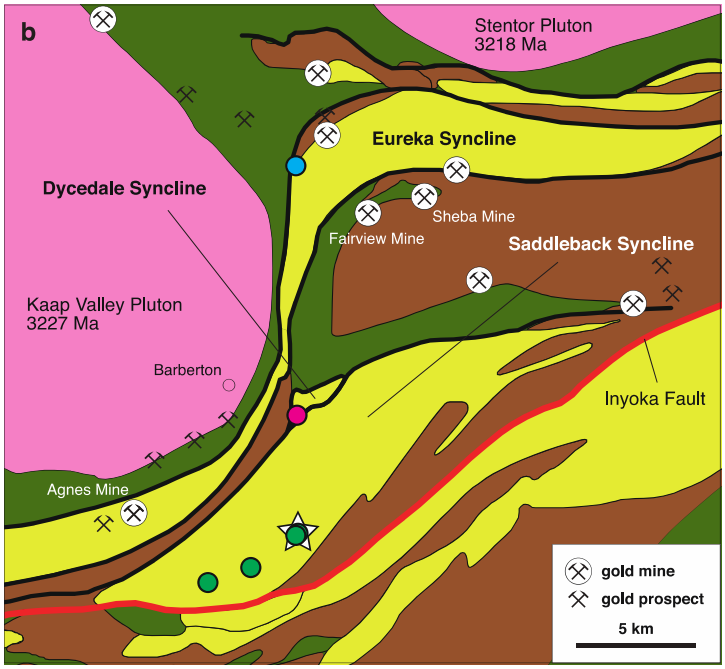

Figure 1. General geology of the Barberton Greenstone Belt (BGB). (**a**) Simplified geological map of the BGB after Homann et al. (2015) and Agangi et al. (2016) [9,29]. The map is an enlargement of the square in the inset. The age of the Stentor Pluton is after Zeh et al. (2009) [30]. (**b**) Closeup of the dashed square in a, after Homann et al. (2015), Heubeck et al. (2016), and Agangi et al. (2019) [9,25,31]. Blue, pink, and green circles show sample localities for SIMS analyses. A star shows the sample locality for IR-MS analyses. Note that there are several gold mines/prospects including the Sheba, Fairview, and Agnes around the sample localities.

3. Lithofacies and Sulfide Description of the Analyzed Rocks

The Moodies conglomerates and sandstones were collected from three synclines north of the Inyoka Fault in the central BGB (Figure 1): the Eureka, Dycedale, and Saddleback synclines. The samples for SIMS analyses were chosen based on the content of microscopically visible sulfide. One sample from the Eureka Syncline (sample 12-007-1: 25°42′4.3″ S, 31°04′46.1″ E) is a conglomerate with a sandstone matrix from the base of unit MdQ1 of the Moodies Group (Figure 2a,b) [5,32]. The conglomerate contains common dolomitic clasts that are likely a rip-up clast from reworked carbonate crusts [33]. The pyrite grains in this conglomerate are mostly euhedral and range in size from 20 to 1000 µm (Figure 3a). The pyrite formed as cement that fills a space between clastic grains and is attached to a grain boundary.

One sample was collected from the Dycedale syncline (sample 14-145: 25°47′34.2″ S, 31°05′22.1″ E; Figure 1b). It consists of a conglomerate with a coarse sandy matrix (Figure 2c,d), from the lower fluvial to alluvial intercalation of coarse-grained sandstone and conglomerate in the basal Moodies deposits of this location (Unit C in Heubeck et al., 2016) [5,28]. Slightly wavy dark and organic rich laminae (possible fossilized microbial mats) are recognized in the conglo merate. This sample contains localized rounded pyrite grains ranging in size mostly from 20 to 200 µm. Large (>500 µm) euhedral pyrite crystals are also included. These pyrite grains occur within the cements aligned along a grain boundary.

Forty-nine samples were collected from the Saddleback Syncline (Figure 1b): three samples for SIMS analyses, 45 for bulk analyses, and one for both. These rocks are quartzose sandstone from unit MdQ1 of the Moodies Group (Figure 2e,f) [5,9]. These samples contain pyrite with euhedral and rounded morphologies that range in size from 10 to 500 µm (Figure 3). Samples for bulk analyses were collected from a ~350 m thick sedimentary succession (base: 25°50′19.9″ S, 31°05′01.1″ E; top: 25°50′13.2″ S, 31°04′53.9″ E) in the Saddleback Syncline (Figure 4). The analyzed succession is close to Log 9 of Homann et al. (2015) [9]. The analyzed rocks are generally composed of medium- to

fine-grained sands of quartz, K-feldspar, and chert [24]. Cross bedding and wavy laminae are commonly observed and the latter is interpreted as fossilized microbial mats (e.g., [8–10,34,35]). Some K-feldspar grains are altered to albite. Micro-quartz and muscovite/sericite cements are common. Titanium- and iron-oxide are also present in the rocks.

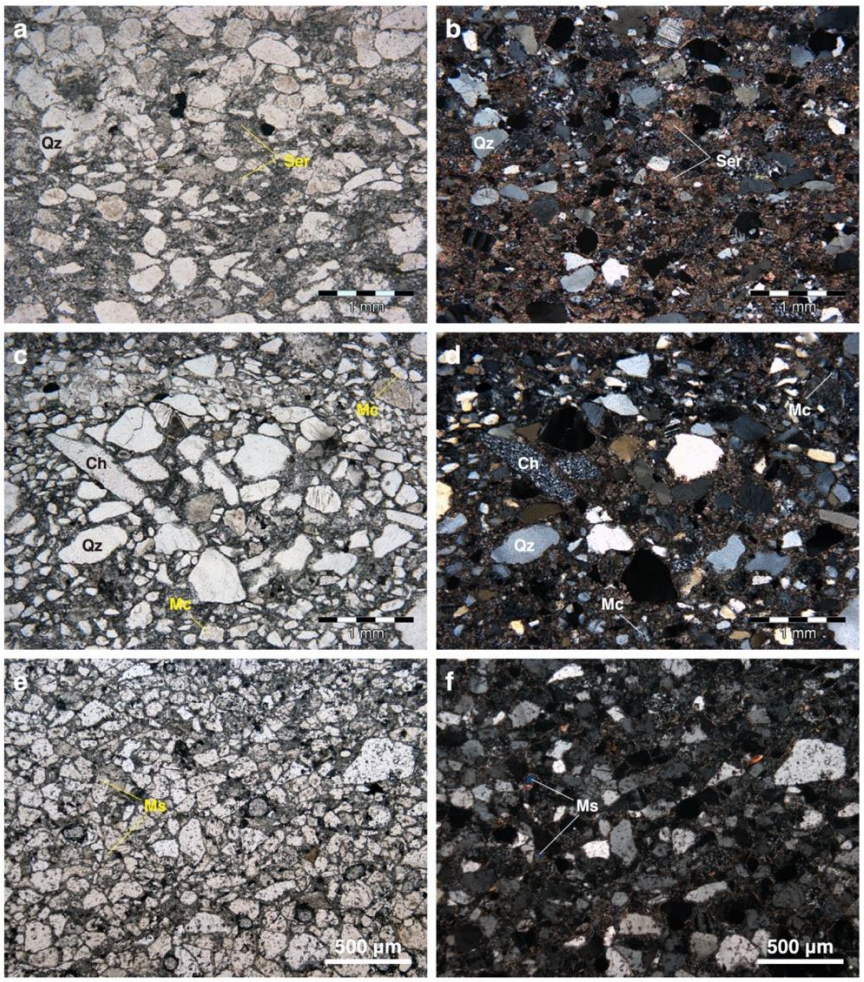

Figure 2. Photomicrographs of the analyzed Moodies rocks from the Eureka (**a**,**b**) (sample 12-007), Dycedale (**c**,**d**) (sample 14-145), and Saddleback (**e**,**f**) (sample SAD22) synclines. Left: Plane light. Right: Polarized light. Qz: quartz; Ch: chert; Mc: microcline; Ms: muscovite.

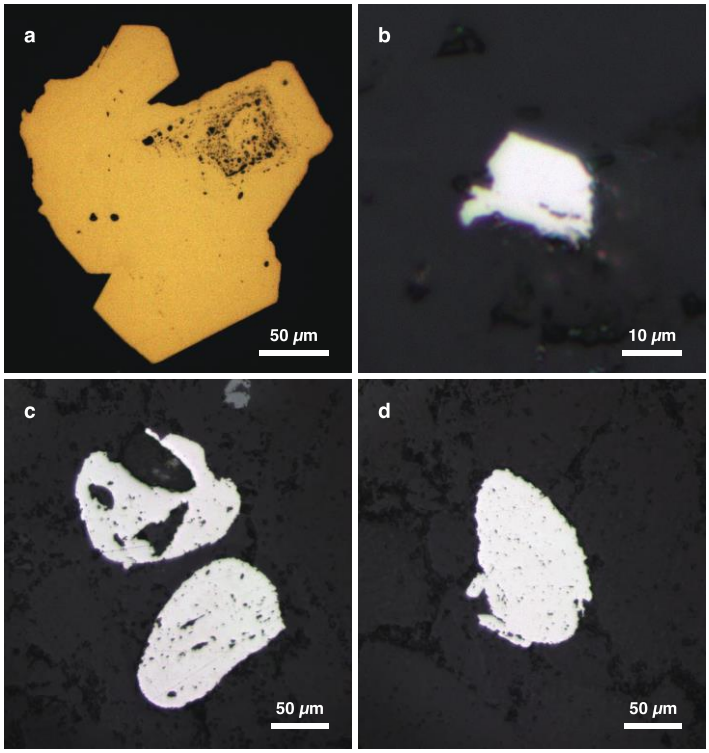

Figure 3. Varied pyrite morphology in the analyzed Moodies rocks. (**a**) Large euhedral pyrite (12-007-1 #3) from the Eureka Syncline. (**b**) Small subhedral pyrite (SAD27 #2) from the Saddleback Syncline. (**c**) Rounded pyrite grains (upper: 11-196 #2-1; lower: 11-196 #2-2) from the Saddleback Syncline. (**d**) Rounded pyrite grain in the sandstone (11-196 #3) from the Saddleback Syncline.

The analyzed Saddleback interval is stratigraphically subdivided into four units following the "Log 9" nomenclature in Homann et al. (2015) (Figure 4) [9,34]. Unit 1 is ~200 m thick and composed of poorly sorted, medium- to fine-grained, cross-bedded and gravelly sandstone. Gamper et al. (2011) and Homann et al. (2015) interpreted Unit 1 as representing a coastal floodplain [9,34]. Unit 2 is ~40 m thick and consists of poorly to moderately sorted, medium-grained sandstone with strings of microbial chip conglomerate. Homann et al. (2015) interpreted this unit as deposited in an intertidal setting. ~80 m thick Unit 3 is composed mainly of medium- to fine-grained sandstone with no laminae [9]. Unit 3 was interpreted as being deposited in a subtidal setting. Unit 4 is ~40 m thick and consists of poorly to moderately sorted, medium-grained sandstone with abundant muscovite/ sericite fabrics. Homann et al. (2015) interpreted that this unit was deposited in upper inter- to supratidal settings [9]. A slight difference in thickness of units 2 and 3 are observed between Log 9 of Homann et al. (2015) and the present log. It could be explained by a lateral change in thickness of megaripple and dune that form these units [9].

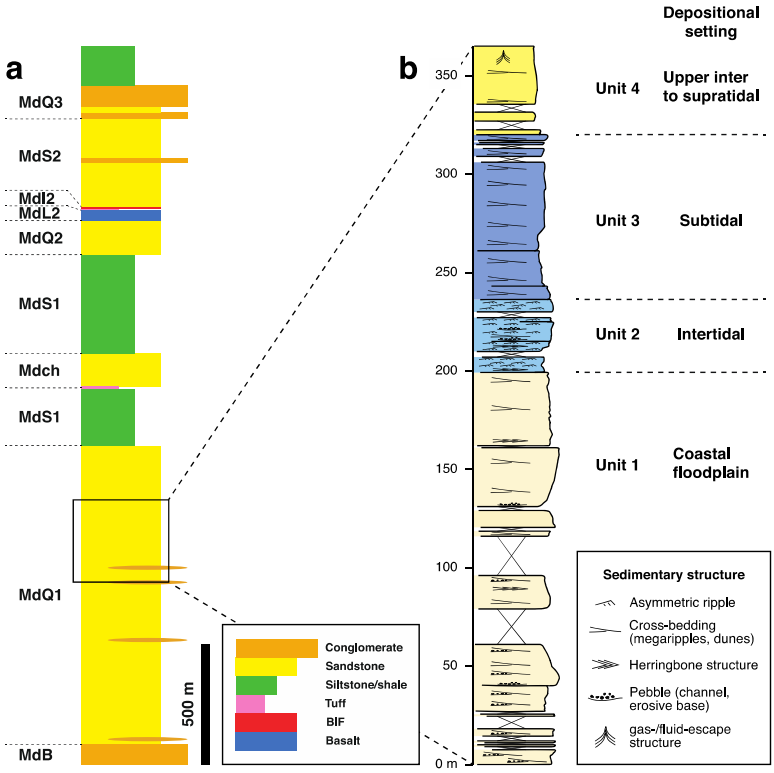

Figure 4. General stratigraphy of the Moodies Group in the Saddleback Syncline (**a**) and the analyzed succession in this study (**b**). The depositional environments are based on interpretations from Homann et al. (2015) [9].

4. Analytical Methods

4.1. Sulfur Isotope Analyses by SIMS

Sulfur isotopes were measured using a Cameca 1280 HR at UNIL in Lausanne, Switzerland, and at CRPG-CNRS in Nancy, France, during two sessions following the analytical protocol described in detail by Whitehouse et al. (2013) and Marin-Carbonne et al. (2014) [36,37]. A Cs^+ primary beam of 5 nA intensity was focused to a spot of about 15–20 µm. Typical $^{32}S^-$ intensity was between 6 and 10×10^8 counts per second (cps) for sulfide. $^{32}S^-$, $^{33}S^-$ and $^{34}S^-$ were measured in multicollection mode with three off-axis Faraday cups. The mass resolution was set to 5000 to resolve the isobaric interferences due to hydride contribution on $^{33}S^-$. A typical analysis consisted of 2 min of pre-sputtering in raster mode followed by data acquisition in 40 cycles of 5 s each. The background of the detectors was measured during the pre-sputtering and was then corrected for each analysis. The internal precision achieved under these conditions was better than 0.05‰ for $\delta^{34}S$ and better than 0.03‰ for $\delta^{33}S$ values (2σ). Several pyrite crystals (Maine: $\delta^{34}S = -20.61$‰, $\delta^{33}S = -10.63$‰; Spain: $\delta^{34}S = -1.56$‰, $\delta^{33}S = -0.78$‰; and Balmat: $\delta^{34}S = +15.84$‰, $\delta^{33}S = +8.12$‰) [38] were used to infer: (1) the instrumental mass fractionation and (2) the reference mass discrimination line, from which $\Delta^{33}S$ values were calculated. The reproducibility was better than ±0.4‰ (2σ) for $\delta^{34}S$ and ±0.1‰ (2σ) for $\Delta^{33}S$ values.

4.2. Sulfur Isotope Analyses by IR-MS

For the 46 samples from the Saddleback succession, we tried to extract sulfide sulfur for isotope analyses by using Isotope Ratio Mass Spectrometry (IR-MS). The rock samples were cut by a disc-saw and weathered surfaces and veins were carefully removed. The slabs were crushed into small chips (<1 cm in diameter) and were ultrasonically rinsed with distilled water and subsequently with pure acetone. The cleaned chips were then powdered using an agate mill. Up to 25 g of bulk powder was

prepared for each sample. Sulfide sulfur was retrieved by using a wet chemical extraction line at the Biogéosciences Laboratory, Dijon, France. Preliminary results of extraction tests and of EPMA analyses suggested that little acid volatile sulfur (AVS) (primarily monosulfide) is contained in the analyzed rocks (Supplementary Table S4). Thus, we retrieved AVS and chromium(II)-reducible sulfur (CRS) (primarily pyrite) together. The AVS and CRS were reduced to hydrogen sulfide (H_2S) and liberated in the deoxygenated line using concentrated HCl and ethanol, and a 1 M $CrCl_2$ solution, respectively [39,40]. The released H_2S was precipitated as silver sulfide (Ag_2S) and was cleaned by repeated centrifugation with deionized distilled water. The residual Ag_2S was dried at 50 °C for >24 h in an oven before gravimetric quantification.

Because the CRS content of the analyzed rocks from the Saddleback Syncline is generally substantially low (<50 ppm), we could analyze the sulfur isotopic composition of CRS for 17 of the 46 samples at the Earth-Life Science Institute (ELSI), Tokyo, Japan. The Ag_2S was wrapped in an iron–nickel–cobalt alloy together with CoF_3 and was converted to sulfur hexafluoride (SF_6) at 590 °C by induction heating with a Curie-point pyrolyzer [41]. The produced SF_6 was purified using a cryogenic technique and gas chromatography. The quadruple isotopic composition of SF_6 was determined using a ThermoFinnigan MAT253 mass spectrometer with a dual inlet system. The sulfur isotopic composition is presented using delta and capital delta notation (formulae 1–3). The $\delta^{34}S$, $\Delta^{33}S$, and $\Delta^{36}S$ values are reported in ‰ relative to the Vienna Canyon Diabro Troilite (V-CDT) international standard. The analytical reproducibility of the $\delta^{34}S$, $\Delta^{33}S$, and $\Delta^{36}S$ values, based on replicate analyses of the international reference material IAEA-S1, is better than ±0.3‰, ±0.01‰, and ±0.1‰ (2σ), respectively.

4.3. Electron Probe Micro Analyzer (EPMA) Analyses

The JEOL JXA 8200 Superprobe at the FU Berlin was used to qualitatively analyze trace element (TE) composition of pyrite crystals in polished thin sections and mounts. Measurements were done using an acceleration voltage of 20 kV and a probe current of 100 nA, resulting in an effective probe diameter of 1 µm. Qualitative trace element mappings for Nickel (Ni) and Cobalt (Co) were conducted on pyrite grains to visualize chemical zoning and to infer detailed morphologies.

5. Results

5.1. Sulfur Isotopic Variation through the Central BGB

The sulfur isotopic composition of 17 samples was measured in bulk, and the composition of 48 pyrite grains in six samples from three synclines were analyzed by SIMS (Supplementary Tables S1–S3). Figures 5 and 6 show frequency histograms and $\delta^{34}S$–$\Delta^{33}S$ cross plots of the whole SIMS dataset. The $\delta^{34}S$ and $\Delta^{33}S$ values of the Moodies samples range mostly between 0‰ and +3‰ and between –0.1‰ and +0.2‰, respectively. In the SIMS data subset, the averaged $\delta^{34}S$ values are +2.3 ± 0.4‰ (1σ, n = 30), +1.5 ± 1.7‰ (1σ, n = 36), and +1.4 ± 2.2‰ (1σ, n = 64) in the Eureka, Dycedale, and Saddleback synclines, respectively (Figure 5a). The averaged $\Delta^{33}S$ values are +0.1 ± 0.1‰ (1σ, n = 30), 0 ± 0.2‰ (1σ, n = 36), and +0.1 ± 0.3‰ (1σ, n = 64) in the Eureka, Dycedale, and Saddleback synclines, respectively (Figure 5b). Although the number of samples from the Eureka and Dycedale synclines is relatively small, the averaged values of three synclines are very close to each other in both $\delta^{34}S$ and $\Delta^{33}S$ values.

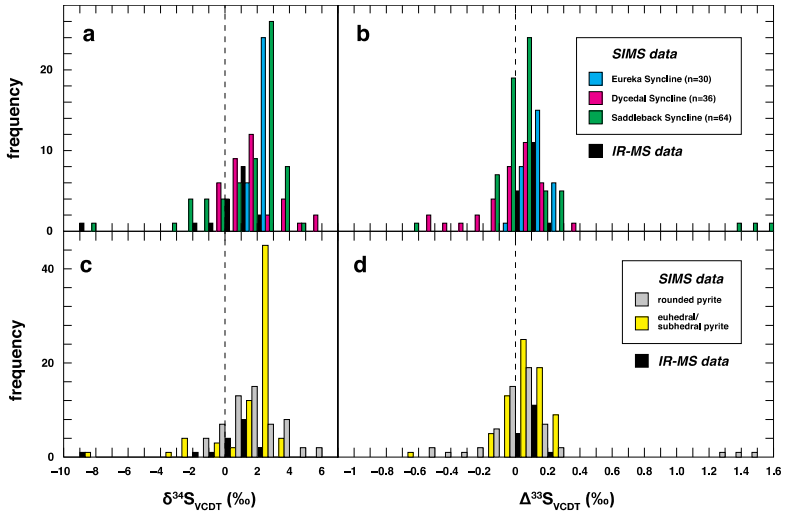

Figure 5. Frequency histogram of multiple sulfur isotope data from the Moodies Group. The $\delta^{34}S$ (**a**) and $\Delta^{33}S$ (**b**) frequencies in the three analyzed synclines. (**c**,**d**) The $\delta^{34}S$ (**c**) and $\Delta^{33}S$ (**d**) frequencies in rounded and euhedral/subhedral pyrite.

The sulfur isotope records of rounded and euhedral/ subhedral pyrite grains are different from each other (Figures 5 and 6). In general, the $\delta^{34}S$ values of euhedral/subhedral pyrite grains are slightly higher than the values of rounded pyrite grains (Figure 5c), although the $\delta^{34}S$ values of pyrite of both morphologies are mostly between 0‰ and +4‰. Some rounded pyrite grains show S-MIF signatures (Figures 5d and 6), and one pyrite grain (11-196 #1) from the Saddleback Syncline particularly shows the highest $\Delta^{33}S$ values of ca. +1.4‰. Moreover, eight rounded pyrite grains from the Dycedale Syncline show negative $\Delta^{33}S$ values (between –0.59 and –0.11‰). The $\Delta^{33}S$ range of euhedral/subhedral pyrite grains is largely overlapped with the range of rounded grains, although the $\Delta^{33}S$ values of euhedral/subhedral grains are less varied than the values of rounded grains. Most of euhedral/subhedral pyrite grains show slightly positive $\Delta^{33}S$ values up to +0.3‰. The SIMS results do not show a recognizable trend in the $\delta^{34}S$–$\Delta^{33}S$ cross plot (Figure 6).

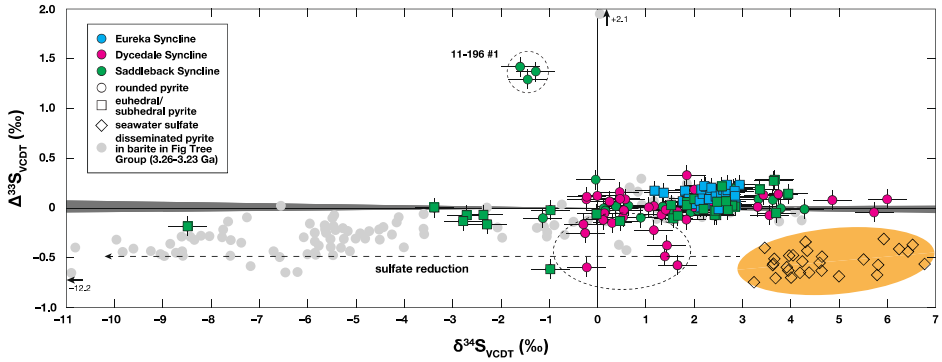

Figure 6. $\delta^{34}S$–$\Delta^{33}S$ cross plot of SIMS data. Error bars are 2SD. A gray field delineates a limit of mass dependent fractionation of sulfur isotopes (S-MDF) from LaFlamme et al. (2018) [17]. A lower dashed circle represents rounded pyrite grains with negative $\Delta^{33}S$ value. The estimated seawater sulfate field (orange circle) is based on Bao et al. (2007) and Roerdink et al. (2012) [42,43]. A dotted line shows the supposed $\delta^{34}S$ range of sulfide produced via biotic/abiotic sulfate reduction. Sulfide data from the slightly older Fig Tree Group in the BGB (light gray dots) for comparison are from Roerdink et al. (2013) [44].

5.2. Sulfur Isotopic Variation in a Chemostratigraphic Profile in the Saddleback Syncline

Figure 7 shows the sulfur chemostratigraphic profiles of the analyzed Saddleback succession. The CRS content is generally low (<50 ppm). The IR-MS $\delta^{34}S$ values are mostly uniform between 0‰ and +2‰ throughout the succession, except for one sample (SAD8) showing a substantially low $\delta^{34}S$ value (−9‰). No systematic isotopic difference between stratigraphic units is recognized. Especially, Unit 3, which does not contain any laminae, displays a similar sulfur isotopic range to the range in the other units that contain frequent laminae.

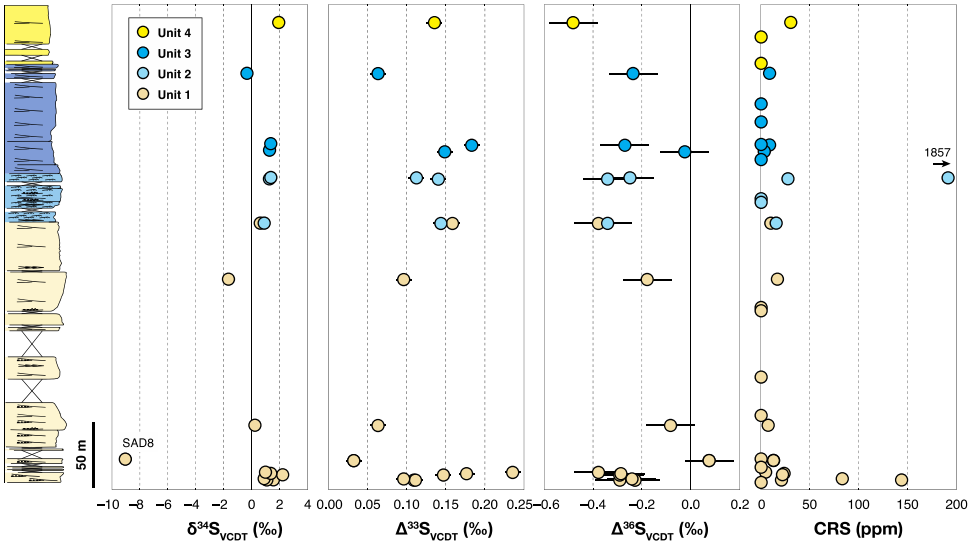

Figure 7. Bulk sulfur chemostratigraphy in the analyzed Saddleback succession. CRS: chromium(II)-reducible sulfur. Error bars are 2SD.

Figure 8 shows $\delta^{34}S$–$\Delta^{33}S$ (a) and $\Delta^{33}S$–$\Delta^{36}S$ (b) cross plots of the IR-MS results. On a $\delta^{34}S$-$\Delta^{33}S$ cross plot, Archean sulfides generally show a positively correlated variation with a slope around +0.9, termed the Archean Reference Array (ARA) [45], which is not recognized in our dataset. In the same manner, on a $\Delta^{33}S$–$\Delta^{36}S$ cross plot, Archean sulfides and sulfates usually show a negatively correlated variation with a slope between −1.5 and −0.9, also termed the ARA [12,14]. These slopes are not reflected in the present Moodies dataset.

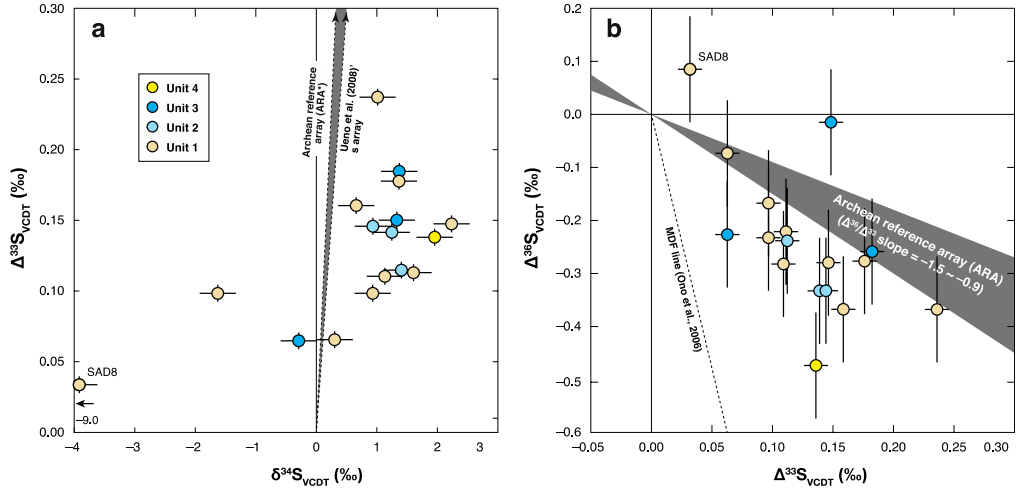

Figure 8. $\delta^{34}S$–$\Delta^{33}S$ (**a**) and $\Delta^{33}S$–$\Delta^{36}S$ (**b**) correlations of IR-MS data. A shaded area in **a** and **b** represents the Archean reference array (ARA). Error bars are 2SD.

The $\delta^{34}S$ and $\Delta^{33}S$ ranges of IR-MS data are generally overlapped with the ranges of rounded and euhedral/subhedral pyrite grains (Figure 5). Thus, the IR-MS results are consistent with the SIMS results. The IR-MS $\Delta^{33}S$ values are all positive up to +0.25‰. Although the SIMS analyses demonstrate that few rounded pyrite grains show negative $\Delta^{33}S$ values (−0.59 to −0.11‰), such a negative S-MIF signal may be obscured in the bulk IR-MS records.

5.3. Sulfur Isotopic Variation within an Indivisual Pyrite Grain

5.3.1. Rounded Pyrite

We measured 30 rounded pyrite grains on two samples (11-196 and 14-145) by SIMS (Supplementary Table S1). In 11 grains we could measure only one point within each grain because of their small size. Only six of the remaining 19 grains show significant intragrain $\delta^{34}S$ variations of up to 3.1‰, by considering the analytical uncertainty of the measurements. Four grains show significant intragrain $\Delta^{33}S$ variations of up to 0.27‰, with the exception of one grain (11-196 #1) that shows a variation of up to 1.13‰. The results show that rounded pyrite grains are isotopically homogeneous in general.

5.3.2. Euhedral/Subhedral Pyrite

We measured 18 euhedral/subhedral pyrite grains by SIMS, and in 8 grains we could measure only one point within each grain because of their small size (Supplementary Table S1). Of the remaining 10 grains, seven show significant intragrain $\delta^{34}S$ variation of up to 5.3‰. Two grains show intragrain $\Delta^{33}S$ variation of up to 0.34‰. Euhedral/subhedral pyrite grains are generally larger than rounded grains (Figure 3), and the number of measured points within an individual euhedral/subhedral grain is significantly larger than the number within a rounded grain (Supplementary Table S1). Therefore, we do not discuss the difference in intragrain $\delta^{34}S$ and $\Delta^{33}S$ variations between rounded and euhedral/subhedral pyrite further in the latter section to avoid the foreseen statistical bias.

6. Discussion

6.1. Rounded Pyrite Origin

The analyzed Moodies rocks frequently contain rounded pyrite grains (Figure 3). Based on their morphology, the rounded pyrite grains are likely of detrital origin. Some rounded pyrite grains show S-MIF (Figure 6) and can therefore be interpreted as reworked detrital pyrite derived from older sedimentary rocks of the Onverwacht and Fig Tree groups [24].

Eight rounded pyrite grains from the Dycedale Syncline show negative $\Delta^{33}S$ values (−0.59 to −0.11‰) (lower dashed circle in Figure 6). Previous studies of Paleoarchean barite records in the BGB ([14,42,43]) suggested that the $\Delta^{33}S$ value of Paleoarchean seawater sulfate around the Kaapvaal Craton was negative, around −0.5‰. It is consistent with the Paleoarchean barite records in Pilbara ([46,47]) and with results of laboratory photochemical experiments [18]. Thus, seawater sulfate was likely a sulfur source of the observed rounded pyrite grains with negative $\Delta^{33}S$ values. The seawater sulfate may have been reduced and the produced sulfide was added to the older Onverwacht and Fig Tree sediments. Both biotic and abiotic processes are possible mechanisms accounting for sulfate reduction in these older sediments. For example, MSR may have occurred during the deposition of older source sediments. The sulfate may have been reduced with $^{34}S/^{32}S$ fractionation factors in the range of 0–10‰ at low sulfate concentration (<200 μM) in the Paleoarchean oceans [48]. Abiotic thermochemical sulfate reduction (TSR) is another possible candidate for seawater sulfate reduction ([45,46]). Within the sediments after deposition, interstitial sulfate may have been reduced by organic matter or Fe^{2+} at temperatures over 100∘C, with $^{34}S/^{32}S$ fractionation up to 20‰ [49]. Although it is difficult to constrain the original reduction processes of seawater sulfate leading to the negative $\Delta^{33}S$ signals observed in the rounded Moodies pyrite, several previous studies suggested the involvement of MSR for some pyrite in the older Onverwacht and Fig Tree groups [44,50–52] (Figure 6). It is consistent with our

interpretation that the Paleoarchean seawater sulfate was a sulfur source of the rounded pyrite with negative $\Delta^{33}S$ values in the Moodies.

One rounded pyrite grain from the Saddleback Syncline (11-196 #1) is unique (Figure 9), because it shows the highest $\Delta^{33}S$ values (up to +1.4‰) of the presented data set. This grain is also likely a reworked detrital pyrite from older sediments. However, one data-point (11-196@7) at the outer rim of the grain shows relatively high $\delta^{34}S$ (0‰) and low $\Delta^{33}S$ (+0.28‰) values compared to other points (Figure 9a). We interpret that this part is an overgrowth rim of the grain [13] and its major sulfur source was metasomatic sulfur derived secondarily from a hydrothermal fluid. This outer rim shows a subhedral shape that supports its in situ precipitation within the Moodies sediments. Some other rounded pyrite grains show a clear absence of S-MIF (Figure 6), which implies that detrital pyrite in the Moodies has various origins. These pyrite grains with no S-MIF signature may have been derived, at least partly, from surrounding intrusive rocks (tonalite-trondhjemite-granodiorite; TTG) or from felsic volcanic rocks of the Fig Tree and Onverwacht groups together with clastic quartz and microcline grains that are major components of the Moodies.

6.2. Euhedral/Subhedral Pyrite Origin

In contrast to rounded pyrite grains of detrital origin, euhedral and subhedral pyrite grains likely precipitated in situ (Figure 3), at least partly [13], within the sediments. Three possible sulfur sources can be considered for these euhedral/subhedral pyrite: (1) seawater sulfate, (2) atmospheric sulfur, and (3) metasomatic sulfur in a hydrothermal fluid. A seawater sulfate pool is a possible sulfur source for the Moodies euhedral/subhedral pyrite, although it should not be a major one. As mentioned in the former section, the $\Delta^{33}S$ value of Paleoarchean seawater sulfate has been suggested to be negative (~−1‰) (Figures 5 and 6). If the seawater sulfate was a major sulfur source of the Moodies euhedral/subhedral pyrite, the negative $\Delta^{33}S$ value should have been recorded in the pyrite, as observed in other Paleoarchean records from the BGB and Pilbara (e.g., [44,46,47]). However, the $\Delta^{33}S$ values of the Moodies pyrite are mostly positive (up to +0.3‰) and therefore do not support its seawater sulfate origin.

S^0 carrying a positive $\Delta^{33}S$ value produced via photochemical reactions of SO_2 in the atmosphere is another possible sulfur source of the euhedral/subhedral pyrite [18]. The atmospheric S^0 may have been reduced by microbial S^0 metabolism, such as S^0 reduction and disproportionation, and have eventually precipitated as sulfide within the sediments. However, the $\Delta^{33}S$ values of euhedral/subhedral pyrite are at most +0.3‰ and are too low to consider photochemically produced S^0 as its major sulfur source (e.g., [53]). The atmospheric S^0 is unlikely a main sulfur source of the euhedral/subhedral pyrite. Together with the former argument about MSR, we conclude that a contribution of sedimentary microbial activity during early diagenesis to euhedral/subhedral pyrite precipitation was not significant in the analyzed Moodies rocks.

Metasomatic sulfur in a hydrothermal fluid is the third possible sulfur source of the Moodies euhedral/subhedral pyrite and is most likely a major one. A circulation of metasomatic fluids during later regional metamorphism may have contributed substantially to the euhedral/subhedral pyrite precipitation (see Figure 6.16 in Heubeck, 2019) [5]. In this scenario, the observed positive $\Delta^{33}S$ values (up to +0.3‰) of most of the euhedral/subhedral pyrite could originate from a small contribution (from a mass balance point of view) of MIF-sulfur recycled by metasomatic fluids from older sedimentary source. Sulfides in several Archean gold deposits in the BGB and in Pilbara, including the Sheba and Fairview gold mines that are close to the present study area (Figure 1b), show S-MIF signatures ($\Delta^{33}S < +1.0$‰) (e.g., [17,54,55]). This suggests that metasomatic fluids on these Archean cratons commonly include recycled sedimentary (i.e., non-juvenile) sulfur derived from older sediments that accumulated on the cratons. It is consistent with a metasomatic origin of the Moodies euhedral/subhedral pyrite with positive $\Delta^{33}S$ values.

Chemical zoning patterns observed within some euhedral pyrite grains (Figure 10) imply repeated fluid injections into the sediments and multiple growth stages of the metasomatic pyrite precipitation.

$\delta^{34}S$ and $\Delta^{33}S$ variations within individual euhedral/subhedral pyrite grains (Figure 9) could be attributed to the multiple stages of crystal growth and/or to minor isotopic fractionation during the fluid circulation in the sediments, such as preferential precipitation and removal of isotopically light sulfide from the fluid. The abundant occurrence of micro-quartz and sericite cements between the clastic grains in the analyzed Moodies rocks (Figure 2) supports a strong influence of metasomatic fluid circulation on secondary mineral precipitation in the sediments. Some K-feldspar grains are affected by albitization, which is also consistent with the metasomatism scenario. The $\Delta^{33}S$ frequency histogram also shows that the $\Delta^{33}S$ values of euhedral/subhedral grains are less varied than the values of rounded grains (Figure 5c). In contrast to the various origins of detrital pyrite as discussed in Section 6.1, we argue that metasomatic sulfur in a fluid was a major sulfur source of the Moodies euhedral/subhedral pyrite.

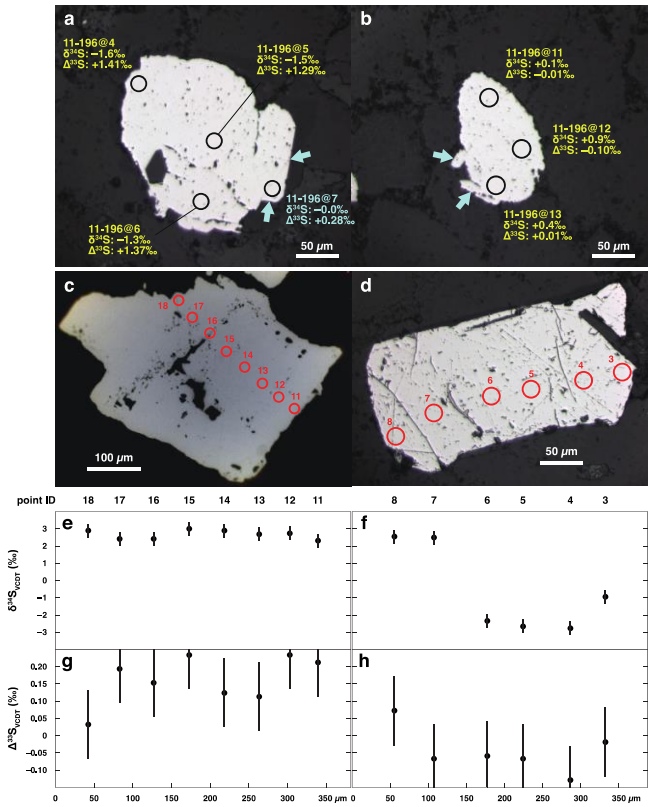

Figure 9. Sulfur isotopic variation within individual pyrite grains. (**a**,**b**) rounded pyrite grains from the Saddleback Syncline (**a**: 11-196 #1; **b**: 11-196 #3). In a, note that the $\delta^{34}S$ and $\Delta^{33}S$ values at 11-196@7 at the outer rim are systematically different from the values of other points. This outer rim shows a subhedral shape (arrows) indicating that this part precipitated in situ secondarily. In b, a protruded part at the outer rim (arrows) may also reflect a secondary overgrowth although it is too small to be analyzed by SIMS. (**c**–**h**) euhedral pyrite grains from the Eureka Syncline (12-007-1 #2; **c**,**e**,**g**), and from the Saddleback Syncline (16-001-1 #1; **d**,**f**,**h**). Error bars are 2SD.

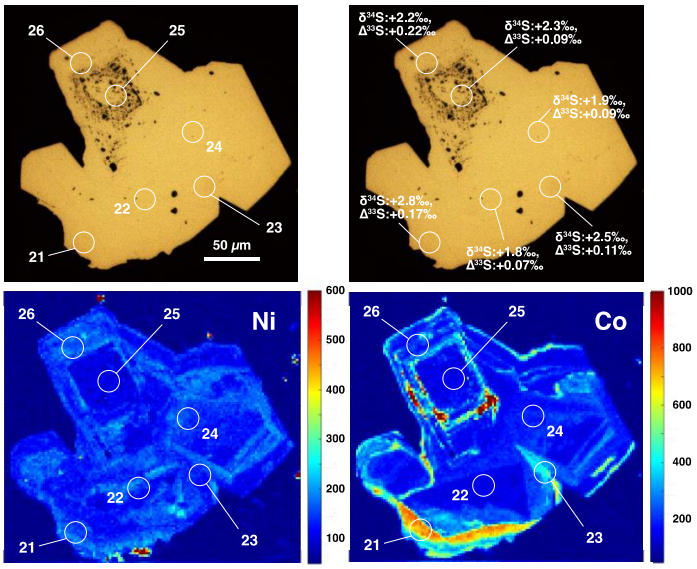

Figure 10. Chemical zoning and $\delta^{34}S$ and $\Delta^{33}S$ variations within a euhedral pyrite grain (12-007-1 #3) from the Eureka Syncline.

6.3. Metasomatic Fluid Circulation at 3.1–3.0 Ga in the Mesoarchean?

The observed similarity of the sulfur isotopic composition of Moodies pyrite from all locations (Figure 5) suggests that late metasomatic pyrite formation occurred commonly north of the Inyoka Fault in the central BGB (Figure 1). Although it is not easy to constrain the timing of the metasomatic pyrite precipitation in the Moodies sediments, several lines of evidence allow us to infer that it occurred in the Mesoarchean between 3.2 and 2.8 Ga. Several gold deposits are known in the northern central BGB, some in close proximity (<10 km) to the analyzed Moodies sections as mentioned above (Figure 1b) [54,55]. Based on rutile and titanite U-Pb ages, these deposits may have been generated at 3.1–3.0 Ga by gold mineralization associated with sulfide precipitation from hydrothermal fluids [31].

Agangi et al. (2016) analyzed the sulfur isotopic composition of sulfide ore by SIMS from the Sheba and Fairview gold mines that are located between the Eureka and Saddleback synclines [29]. The authors reported $\Delta^{33}S$ values of up to +1.0‰ and concluded that the MIF-sulfur that was leached from older volcano-sedimentary successions was a sulfur source of this ore. Their conclusion is consistent with our former interpretation that MIF-sulfur recycled by metasomatic fluids was a sulfur source of euhedral/subhedral pyrite in the Moodies. Moreover, the $\Delta^{33}S$ frequency histogram of the gold deposits is consistent with that of the Moodies pyrite (Figure 11). We infer that metasomatic sulfur derived from fluids at 3.1–3.0 Ga formed the secondary pyrite in the Moodies sediments, associated with the nearby gold mineralization [31]. The $\delta^{34}S$ values of the ore sulfides at Sheba and Fairview are mostly between +4‰ and +5‰ [29] and are slightly higher than the values of the Moodies pyrite (mostly +1‰ to +3‰). This $\delta^{34}S$ difference could be attributed to small isotopic fractionation during fluid circulation in this area (e.g., preferential precipitation and removal of isotopically-light sulfide from the fluid).

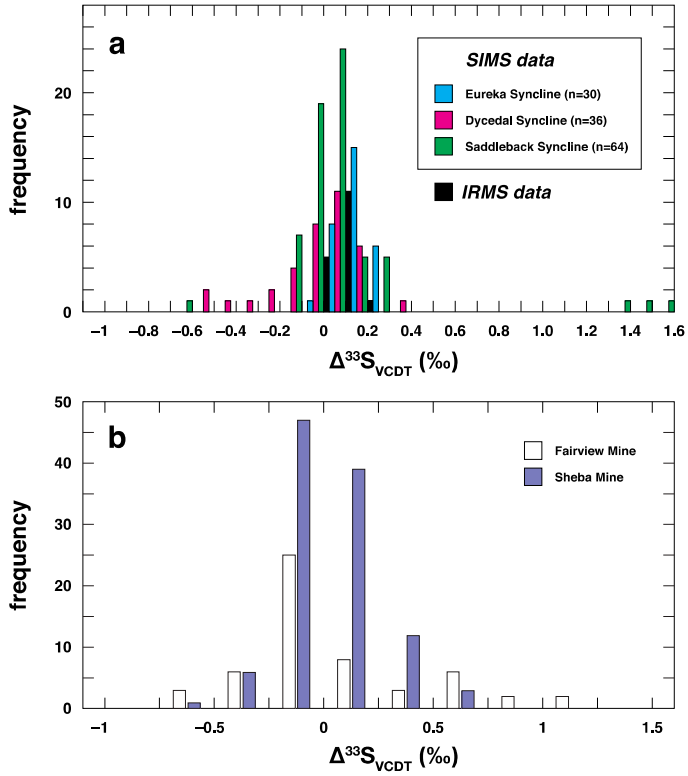

Figure 11. $\Delta^{33}S$ histograms of sulfides in the central BGB. (**a**) The present Moodies data. (**b**) The gold mine data from [29].

6.4. Sulfur Isotope Records of the Moodies Group in the Paleoarchean

Considering all Paleoarchean sulfur records, the analyzed Moodies sediments are characterized by a comparatively low sulfide content (largely <50 ppm) and small range of $\Delta^{33}S$ values (largely –0.5‰ < $\Delta^{33}S$ < +0.5‰) (Figures 5–7). In comparison, the sulfide content of the Onverwacht and Fig Tree rocks is mostly >100 ppm (Supplementary Table S5). Moreover, $\Delta^{33}S$ values of Onverwacht and Fig Tree sulfides analyzed by IR-MS are up to +3.2‰ (Figure 12) [56]. Based on the global database of previously-published Paleoarchean sulfur isotope records [57], statistic t-tests demonstrate that the $\Delta^{33}S$ values of Moodies sulfides are significantly lower than the values of sulfide of most of the Onverwacht and Fig Tree groups. For example, the average $\Delta^{33}S$ value of the present Moodies SIMS data set (+0.06‰, n = 130) is significantly lower than the average value of a SIMS data set from the 3.34 Ga Kromberg Formation of the Onverwacht Group [52] (+0.74‰, n = 49) (p-value < 0.05%).

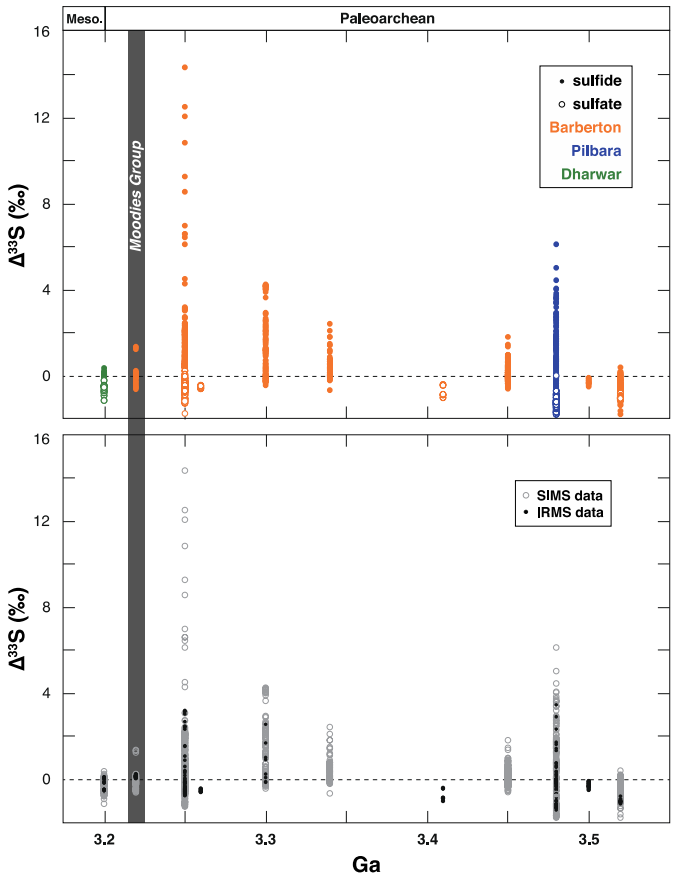

Figure 12. Paleoarchean $\Delta^{33}S$ record. Meso.: Mesoarchean. The data are from [12,13,38,42–44,46,47,52,53,56–66] and this study.

As discussed in Section 6.1, a high flux of detrital pyrite from intrusive and volcanic rocks into the Moodies sediments may have contributed to obscure an atmospheric S-MIF signal. Iron oxides are sometimes observed in the analyzed Moodies rocks. These oxides may be a product of modern oxidative weathering of pyrite [5]. Although such a meteoric weathering process may also have contributed to the low sulfide content (largely <50 ppm) of Moodies, the $\delta^{34}S$ and $\Delta^{33}S$ values of sulfide should have been only slightly changed during the meteoric sulfide oxidation [67]. In a more speculative way, the peculiar characteristic of the Moodies sulfur record can also reflect a very high sediment accumulation rate (~0.1–1 mm/year) [6]. Such fast-accumulated sediments may have prevented the accumulation of sulfur derived from an atmospheric source during their deposition. As a result, the atmospheric derived sulfur content of the initial sediments might have been low, and the sulfur isotopic composition of the sediments became more susceptible to secondary addition of late metasomatic sulfur. Nonetheless, this interpretation is solely a possible scenario without strong evidence for it so far, and the relationship between the fast sedimentation and sulfur records of Moodies should be further examined by future studies.

We emphasize that the present sulfur isotope record is from stratigraphically limited intervals of the lower Moodies Group from three synclines within the central BGB. It is possible that Moodies sedimentary rocks from different stratigraphic intervals or locations have different syn- and post-depositional histories and that different S-MIF signals could be retained in other Moodies intervals. Future analyses of fresh drill core samples from extensive areas in the BGB and data comparison with the present outcrop results would be useful to further reconstruct the syn- and post-depositional history of the entire Moodies Group [5] and help to better uncover the Paleoarchean sulfur cycle.

7. Conclusions

The multiple sulfur isotopic composition of sulfide of the 3.22 Ga Moodies Group in the Barberton Greenstone Belt (BGB) was analyzed in relation to the sedimentological and post-depositional history of the samples. Sandstone and conglomerate samples were collected from three synclines north of the Inyoka Fault in the central BGB: the Eureka, Dycedale, and Saddleback synclines. The $\delta^{34}S$ and $\Delta^{33}S$ values were measured for 6 samples from three synclines by using Secondary Ion Mass Spectrometry (SIMS), and the quadruple sulfur isotopic composition was analyzed for 17 samples from the Saddleback Syncline by using Isotope Ratio Mass Spectrometry (IR-MS). The results show mass-independent fractionation of sulfur isotopes (S-MIF), although the Moodies S-MIF signal (mostly $0‰ < \Delta^{33}S < +0.5‰$) is substantially small compared to the signal of the older Paleoarchean (3.6–3.2 Ga) records. It is argued to reflect (i) detrital pyrite flux from sedimentary and felsic volcanic rocks of the Onverwacht and Fig Tree groups and from surrounding intrusive rocks; (ii) a high accumulation rate of the Moodies sediments; and (iii) secondary addition of metasomatic sulfur. Furthermore, the similarity of sulfur isotopic variation between the present Moodies and surrounding gold deposits implies a common metasomatic sulfide precipitation around 3.1–3.0 Ga in the central BGB.

Supplementary Materials: The following are available online at http://www.mdpi.com/2076-3263/10/4/145/s1, Table S1: The present SIMS data. Table S2: The present IR-MS data of the Saddleback succession. Table S3: The raw isotope data of the SIMS session. Table S4: Preliminary EPMA analyses of Saddleback sulfides. Table S5: The sulfide contents in the Onverwacht and Fig Tree groups.

Author Contributions: Conceptualization, C.T., N.O., S.N., and J.M.-C.; fieldwork and sampling, S.N., N.O., C.T., J.-F.M., and J.M.-C.; lithofacies description, M.S., S.N., and N.O.; bulk isotope measurements, M.S., C.T., and Y.U.; SIMS isotope measurements, M.S., S.N., and J.M.-C.; writing—original draft preparation, M.S., S.N., N.O., C.T., and J.M.-C. All authors have read and agreed to the published version of the manuscript.

Funding: This research was funded by the INSU Programme National de Planetologie, the European Union's Horizon H2020 research and innovation program ERC (STROMATA, grant agreement 759289, J.M.C), the Europlanet 2020 RI TA Programme, (grant number 17-EPN3-074, S.N.), the French Government Laboratory of Excellence initiative (n°ANR-10-LABX-0006), the Fondation Herbette UNIL, the PHC Protea (Campus-France), and the Région Auvergne and the European Regional Development Fund. This is Laboratory of Excellence ClerVolc contribution number 395.

Acknowledgments: Christoph Heubeck and Martin Homann assisted with locating the sampling section. Moritz Mühlberg assisted with the sampling. Nordine Bouden, Etienne Deloule, Anne-Sophie Bouvier and Florent Plane are thanked for their help during the SIMS analytical session. Mayuko Nakagawa assisted with the IR-MS analyses. Christoph Heubeck, Marion Garçon, Paul Mason, and one anonymous reviewer gave us fruitful comments on the early version of the manuscript.

Conflicts of Interest: The authors declare no conflicts of interest.

References

1. Eriksson, K.A.; Simpson, E.L. Quantifying the oldest tidal record: The 3.2 Ga Moodies Group, Barberton Greenstone Belt, South Africa. *Geology* **2000**, *28*, 831–834. [CrossRef]
2. Eriksson, K.A.; Simpson, E.L.; Mueller, W. An unusual fluvial to tidal transition in the mesoarchean Moodies Group, South Africa: A response to high tidal range and active tectonics. *Sediment. Geol.* **2006**, *190*, 13–24. [CrossRef]
3. Simpson, E.L.; Eriksson, K.A.; Mueller, W.U. 3.2 Ga eolian deposits from the Moodies Group, Barberton Greenstone Belt, South Africa: Implications for the origin of first-cycle quartz sandstones. *Precambrian Res.* **2012**, *214–215*, 185–191. [CrossRef]
4. Lowe, D.R.; Byerly, G.R.; Heubeck, C. Structural divisions and development of the west-central part of the Barberton Greenstone Belt. In *Geologic Evolution of the Barberton Greenstone Belt, South Africa*; Lowe, D.R., Byerly, G.R., Eds.; Geological Society of America: Boulder, CO, USA, 1999; pp. 37–82.
5. Heubeck, C. The Moodies Group—A High-Resolution Archive of Archaean Surface Processes and Basin-Forming Mechanisms. In *The Archaean Geology of the Kaapvaal Craton, Southern Africa*; Kröner, A., Hofmann, A., Eds.; Springer Nature Switzerland AG: Cham, Switzerland, 2019; pp. 133–169.

6. Heubeck, C.; Engelhardt, J.; Byerly, G.R.; Zeh, A.; Sell, B.; Luber, T.; Lowe, D.R. Timing of deposition and deformation of the Moodies Group (Barberton Greenstone Belt, South Africa): Very-high-resolution of Archaean surface processes. *Precambrian Res.* **2013**, *231*, 236–262. [CrossRef]
7. Noffke, N.; Eriksson, K.A.; Hazen, R.M.; Edward, L.; Simpson, E.L. A new window into Early Archean life: Microbial mats in Earth's oldest siliciclastic tidal deposits (3.2 Ga Moodies Group, South Africa). *Geology* **2006**, *34*, 253–256. [CrossRef]
8. Heubeck, C. An early ecosystem of Archean tidal microbial mats (Moodies Group, South Africa, ca. 3.2 Ga). *Geology* **2009**, *37*, 931–934. [CrossRef]
9. Homann, M.; Heubeck, C.; Airo, A.; Tice, M.M. Morphological adaptations of 3.22 Ga-old tufted microbial mats to Archean coastal habitats (Moodies Group, Barberton Greenstone Belt, South Africa). *Precambrian Res.* **2015**, *266*, 47–64. [CrossRef]
10. Homann, M.; Sansjofre, P.; Van Zuilen, M.; Heubeck, C.; Gong, J.; Killingsworth, B.; Foster, I.S.; Airo, A.; Van Kranendonk, M.J.; Ader, M.; et al. Microbial life and biogeochemical cycling on land 3220 million years ago. *Nat. Geosci.* **2018**, *11*, 665–671. [CrossRef]
11. Johnston, D.T. Multiple sulfur isotopes and the evolution of Earth's surface sulfur cycle. *Earth Sci. Rev.* **2011**, *106*, 161–183. [CrossRef]
12. Farquhar, J.; Peters, M.; Johnston, D.T.; Strauss, H.; Masterson, A.; Wiechert, U.; Kaufman, A.J. Isotopic evidence for Mesoarchaean anoxia and changing atmospheric sulphur chemistry. *Nature* **2007**, *449*, 706–709. [CrossRef]
13. Nabhan, S.; Wiedenbeck, M.; Milke, R.; Heubeck, C. Biogenic overgrowth on detrital pyrite in ca. 3.2 Ga Archean paleosols. *Geology* **2016**, *44*, 763–766. [CrossRef]
14. Farquhar, J.; Bao, H.; Thiemens, M. Atmospheric influence of Earth's earliest sulfur cycle. *Science* **2000**, *289*, 756–758. [CrossRef] [PubMed]
15. Farquhar, J.; Wing, B.A. Multiple sulfur isotopes and the evolution of the atmosphere. *Earth Planet. Sci. Lett.* **2003**, *213*, 1–13. [CrossRef]
16. Ono, S.; Wing, B.; Johnston, D.; Farquhar, J.; Rumble, D. Mass-dependent fractionation of quadruple stable sulfur isotope system as a new tracer of sulfur biogeochemical cycles. *Geochim. Cosmochim. Acta* **2006**, *70*, 2238–2252. [CrossRef]
17. LaFlamme, C.; Jamieson, J.W.; Fiorentini, M.L.; Thébaud, N.; Caruso, S.; Selvaraja, V. Investigating sulfur pathways through the lithosphere by tracing mass independent fractionation of sulfur to the Lady Bountiful orogenic gold deposit, Yilgarn Craton. *Gondwana Res.* **2018**, *58*, 27–38. [CrossRef]
18. Farquhar, J.; Savarino, J.; Airieau, S.; Thiemens, M.H. Observation of wavelength-sensitive mass-independent sulfur isotope effects during S02 photolysis: Implications for the early atmosphere. *J. Geophys. Res.* **2001**, *106*, 32829–32839. [CrossRef]
19. Masterson, A.L.; Farquhar, J.; Wing, B.A. Sulfur mass-independent fractionation patterns in the broadband UV photolysis of sulfur dioxide: Pressure and third body effects. *Earth Planet. Sci. Lett.* **2011**, *306*, 253–260. [CrossRef]
20. Ono, S.; Whitehill, A.R.; Lyons, J.R. Contribution of isotopologue self-shielding to sulfur mass-independent fractionation during sulfur dioxide photolysis. *J. Geophys. Res.* **2013**, *118*, 2444–2454. [CrossRef]
21. Ono, S. Photochemistry of sulfur dioxide and the origin of mass-independent isotope fractionation in Earth's atmosphere. *Annu. Rev. Earth Planet. Sci.* **2017**, *45*, 301–329. [CrossRef]
22. Ono, S.; Kaufman, A.J.; Farquhar, J.; Sumner, D.Y.; Beukes, N.J. Lithofacies control on multiple-sulfur isotope records and Neoarchean sulfur cycles. *Precambrian Res.* **2009**, *169*, 58–67. [CrossRef]
23. Hofmann, A. The geochemistry of sedimentary rocks from the Fig Tree Group, Barberton greenstone belt: Implications for tectonic, hydrothermal and surface processes during mid-Archaean times. *Precambrian Res.* **2005**, *143*, 23–49. [CrossRef]
24. Heubeck, C.; Lowe, D.R. Sedimentary petrography and provenance of the Archean Moodies Group, Barberton Greenstone Belt. In *Geologic Evolution of the Barberton Greenstone Belt, South Africa*; Lowe, D.R., Byerly, G.R., Eds.; Geological Society of America: Boulder, CO, USA, 1999; pp. 259–286.
25. Anhaeusser, C.R.; Robb, L.J.; Viljoen, M.J. Provisional Geological Map of the Barberton Greenstone Belt and Surrounding Granitic Terrane, Eastern Transvaal and Swaziland (1:250000). 1981. Available online: https://www.worldcat.org/title/provisional-geological-map-of-the-barberton-greenstone-belt-and-surrounding-granitic-terrane-eastern-transvaal-and-swaziland/oclc/79698130 (accessed on 16 April 2020).

26. Heubeck, C.; Lowe, D.R. Late syndepositional deformation and detachment tectonics in the Barberton Greenstone-Belt, South-Africa. *Tectonics* **1994**, *13*, 1514–1536. [CrossRef]
27. Lowe, D.R. Accretionary history of the Archean Barberton Greenstone Belt (3.55–3.22 Ga), southern Africa. *Geology* **1994**, *22*, 1099–1102. [CrossRef]
28. Heubeck, C.; Bläsing, S.; Grund, M.; Drabon, N.; Homann, M.; Nabhan, S. Geological constraints on Archean (3.22 Ga) coastal-zone processes from the Dycedale Syncline, Barberton Greenstone Belt. *S. Afr. J. Geol.* **2016**, *119*, 495–518. [CrossRef]
29. Agangi, A.; Hofmann, A.; Eickmann, B.; Marin-Carbonne, J.; Reddy, S.M. An atmospheric source of S in Mesoarchaean structurally-controlled gold mineralisation of the Barberton Greenstone Belt. *Precambrian Res.* **2016**, *285*, 10–20. [CrossRef]
30. Zeh, A.; Gerdes, A.; Barton, J.M., Jr. Archean accretion and crustal evolution of the Kalahari Craton–the zircon age and Hf isotope record of granitic rocks from Barberton/Swaziland to the Francistown Arc. *J. Petrol.* **2009**, *50*, 933–966. [CrossRef]
31. Agangi, A.; Hofmann, A.; Eickmann, B.; Marin-Carbonne, J. Mesoarchaean Gold Mineralisation in the Barberton Greenstone Belt: A Review. In *The Archaean Geology of the Kaapvaal Craton, Southern Africa*; Kröner, A., Hofmann, A., Eds.; Springer Nature Switzerland AG: Cham, Switzerland, 2019; pp. 171–184.
32. Anhaeusser, C.R. The geology of the Sheba Hills area of the Barberton Mountain Land, South Africa: With particular reference to the Eureka Syncline. *Trans. Geol. Soc. S. Afr.* **1976**, *79*, 253–280.
33. Nabhan, S.; Luber, T.; Scheffler, F.; Heubeck, C. Climatic and geochemical implications of Archean pedogenic gypsum in the Moodies Group (~3.2 Ga), Barberton Greenstone Belt, South Africa. *Precambrian Res.* **2016**, *275*, 119–134. [CrossRef]
34. Gamper, A.; Heubeck, C.; Demske, D.; Hoehse, M. Composition and microfacies of Archean microbial mats (Moodies Group, ca. 3.22 Ga, South Africa). *SEPM Spec. Pub.* **2011**, *101*, 65–74.
35. Köhler, I.; Heubeck, C. Microbial-mat-associated tephra of the Archean Moodies Group, Barberton Greenstone Belt (BGB), South Africa: Resemblance to potential biostructures and ecological implications. *S. Afr. J. Geol.* **2019**. [CrossRef]
36. Whitehouse, M.J. Multiple Sulfur Isotope Determination by SIMS: Evaluation of Reference Sulfides for Δ33S with Observations and a Case Study on the Determination of Δ36S. *Geostand. Geoanal. Res.* **2013**, *37*, 19–33. [CrossRef]
37. Marin-Carbonne, J.; Rollion-Bard, C.; Bekker, A.; Rouxel, O.; Agangi, A.; Cavalazzi, B.; Wohlgemuth-Ueberwasser, C.C.; Hofmann, A.; McKeegan, K.D. Coupled Fe and S isotope variations in pyrite nodules from Archean shale. *Earth Planet. Sci. Lett.* **2014**, *392*, 67–79. [CrossRef]
38. Muller, É.; Philippot, P.; Rollion-Bard, C.; Cartigny, P.; Assayag, N.; Marin-Carbonne, J.; Mohan, M.R.; Sarma, D.S. Primary sulfur isotope signatures preserved in high-grade Archean barite deposits of the Sargur Group, Dharwar Craton, India. *Precambrian Res.* **2017**, *295*, 38–47. [CrossRef]
39. Canfield, D.E.; Raiswell, R.; Westrich, J.T.; Reaves, C.M.; Berner, R.A. The use of chromium reduction in the analysis of reduced inorganic sulfur in sediments and shale. *Chem. Geol.* **1986**, *54*, 149–155. [CrossRef]
40. Gröger, J.; Franke, J.; Hamer, K.; Schulz, H.D. Quantitative recovery of elemental sulfur and improved selectivity in a chromium-reducible sulfur distillation. *Geostand. Geoanal. Res.* **2009**, *33*, 17–27.
41. Ueno, Y.; Aoyama, S.; Endo, Y.; Matsu'ura, F.; Foriel, J. Rapid quadruple sulfur isotope analysis at the sub-micromole level by a flash heating with CoF3. *Chem. Geol.* **2015**, *419*, 29–35. [CrossRef]
42. Bao, H.; Rumble, D., III; Lowe, D.R. The five stable isotope compositions of Fig Tree barites: Implications on sulfur cycle in ca. 3.2 Ga oceans. *Geochim. Cosmochim. Acta* **2007**, *71*, 4868–4879. [CrossRef]
43. Roerdink, D.L.; Mason, P.R.D.; Farquhar, J.; Reimer, T. Multiple sulfur isotopes in Paleoarchean barites identify an important role for microbial sulfate reduction in the early marine environment. *Earth Planet. Sci. Lett.* **2012**, *331–332*, 177–186. [CrossRef]
44. Roerdink, D.L.; Mason, P.R.D.; Whitehouse, M.J.; Reimer, T. High-resolution quadruple sulfur isotope analyses of 3.2 Ga pyrite from the Barberton Greenstone Belt in South Africa reveal distinct environmental controls on sulfide isotopic arrays. *Geochim. Cosmochim. Acta* **2013**, *117*, 203–215. [CrossRef]
45. Ono, S.; Eigenbrode, J.L.; Pavlov, A.A.; Kharecha, P.; Rumble, D.; Kasting, J.F.; Freeman, K.H. New insights into Archean sulfur cycle from mass-independent sulfur isotope records from the Hamersley Basin, Australia. *Earth Planet. Sci. Lett.* **2003**, *213*, 15–30. [CrossRef]

46. Ueno, Y.; Ono, S.; Rumble, D.; Maruyama, S. Quadruple sulfur isotope analysis of ca. 3.5 Ga Dresser Formation: New evidence for microbial sulfate reduction in the early Archean. *Geochim. Cosmochim. Acta* **2008**, *72*, 5675–5691. [CrossRef]
47. Shen, Y.; Farquhar, J.; Masterson, A.; Kaufman, A.J.; Buick, R. Evaluating the role of microbial sulfate reduction in the early Archean using quadruple isotope systematics. *Earth Planet. Sci. Lett.* **2009**, *279*, 383–391. [CrossRef]
48. Habicht, K.S.; Gade, M.; Thamdrup, B.; Berg, P.; Canfield, D.E. Calibration of Sulfate Levels in the Archean Ocean. *Science* **2002**, *298*, 2372–2374. [CrossRef]
49. Machel, H.G. Bacterial and thermochemical sulfate reduction in diagenetic settings—Old and new insights. *Sediment. Geol.* **2001**, *140*, 143–175. [CrossRef]
50. Ohmoto, H.; Goldhaber, M.B. Sulfur and carbon isotopes. In *Geochemistry of Hydrothermal Ore Deposits*; Barnes, H.L., Ed.; John Wiley & Sons: New York, NY, USA, 1997; pp. 517–612.
51. Machel, H.G.; Krouse, H.R.; Sassen, R. Products and distinguishing criteria of bacterial and thermochemical sulfate reduction. *Appl. Geochem.* **1995**, *10*, 373–389. [CrossRef]
52. Grosch, E.G.; McLoughlin, N. Paleoarchean sulfur cycle and biogeochemical surface conditions on the early Earth, Barberton, South Africa. *Earth Planet. Sci. Lett.* **2013**, *377–378*, 142–154. [CrossRef]
53. Philippot, P.; Van Zuilen, M.; Lepot, K.; Thomazo, C.; Farquhar, J.; Van Kranendonk, M.J. Early Archaean microorganisms preferred elemental sulfur, not sulfate. *Science* **2007**, *317*, 1534–1537. [CrossRef]
54. Selvaraja, V.; Caruso, S.; Fiorentini, M.L.; LaFlamme, C.K.; Bui, T.H. Atmospheric sulfur in the orogenic gold deposits of the Archean Yilgarn Craton, Australia. *Geology* **2017**, *45*, 691–694. [CrossRef]
55. Munyai, M.R.; Dirks, P.H.G.M.; Charlesworth, E.G. Archaean gold mineralisation during post-orogenic extension in the New Consort gold mine, Barberton Greenstone Belt, South Africa. *S. Afr. J. Geol.* **2011**, *114*, 121–144. [CrossRef]
56. Montinaro, A.; Strauss, H.; Mason, P.R.D.; Roerdink, D.; Muünker, C.; Schwarz-Schampera, U.; Arndt, N.T.; Farquhar, J.; Beukes, N.J.; Gutzmer, J.; et al. Paleoarchean sulfur cycling: Multiple sulfur isotope constraints from the Barberton Greenstone Belt, South Africa. *Precambrian Res.* **2015**, *267*, 311–322. [CrossRef]
57. The Global Sedimentary Sulfur Isotope Database (GSSID). Available online: http://www.cet.edu.au/research-projects/special-projects/gssid-global-sedimentary-sulfur-isotope-database (accessed on 22 March 2020).
58. Roerdink, D.L.; Mason, P.R.D.; Whitehouse, M.J.; Brouwer, F.M. Reworking of atmospheric sulfur in a Paleoarchean hydrothermal system at Londozi, Barberton Greenstone Belt, Swaziland. *Precambrian Res.* **2016**, *280*, 195–204. [CrossRef]
59. Philippot, P.; van Zuilen, M.; Rollion-Bard, C. Variations in atmospheric sulphur chemistry on early Earth linked to volcanic activity. *Nat. Geosci.* **2012**, *5*, 668–674. [CrossRef]
60. van Zuilen, M.A.; Philippot, P.; Whitehouse, M.J.; Lepland, A. Sulfur isotope mass-independent fractionation in impact deposits of the 3.2 billion-year-old Mapepe Formation, Barberton Greenstone Belt, South Africa. *Geochim. Cosmochim. Acta* **2014**, *142*, 429–441. [CrossRef]
61. Wacey, D.; Noffke, N.; Cliff, J.; Barley, M.E.; Farquhar, J. Micro-scale quadruple sulfur isotope analysis of pyrite from the~3480 Ma Dresser Formation: New insights into sulfur cycling on the early Earth. *Precambrian Res.* **2015**, *258*, 24–35. [CrossRef]
62. Muller, É.; Philippot, P.; Rollion-Bard, C.; Cartigny, P. Multiple sulfur-isotope signatures in Archean sulfates and their implications for the chemistry and dynamics of the early atmosphere. *Proc. Natl. Acad. Sci. USA* **2016**, *113*, 7432–7437. [CrossRef] [PubMed]
63. Aoyama, S.; Ueno, Y. Multiple sulfur isotope constraints on microbial sulfate reduction below an Archean seafloor hydrothermal system. *Geobiology* **2017**, *16*, 107–120. [CrossRef] [PubMed]
64. Galić, A.; Mason, P.R.D.; Mogollón, J.M.; Wolthers, M.; Vroon, P.Z.; Whitehouse, M.J. Pyrite in a sulfate-poor Paleoarchean basin was derived predominantly from elemental sulfur: Evidence from 3.2 Ga sediments in the Barberton Greenstone Belt, Kaapvaal Craton. *Chem. Geol.* **2017**, *449*, 135–146. [CrossRef]
65. Mishima, K.; Yamazaki, R.; Satish-Kumar, M.; Ueno, Y.; Hokada, T.; Toyoshima, T. Multiple sulfur isotope geochemistry of Dharwar Supergroup, Southern India: Late Archean record of changing atmospheric chemistry. *Earth Planet. Sci. Lett.* **2017**, *464*, 69–83. [CrossRef]

66. Busigny, V.; Marin-Carbonne, J.; Muller, E.; Cartigny, P.; Rollion-Bard, C.; Assayag, N.; Philippot, P. Iron and sulfur isotope constraints on redox conditions associated with the 3.2 Ga barite deposits of the Mapepe Formation (Barberton Greenstone Belt, South Africa). *Geochim. Cosmochim. Acta* **2017**, *210*, 247–266. [CrossRef]
67. Thurston, R.S.; Mandernack, K.W.; Shanks III, W.C. Laboratory chalcopyrite oxidation by Acidithiobacillus ferrooxidans: Oxygen and sulfur isotope fractionation. *Chem. Geol.* **2010**, *269*, 252–261. [CrossRef]